International Journal of Research
Available at https://edupediapublications.org/journals
e-ISSN: 2348-6848
p-ISSN: 2348-795X
Volume 04 Issue-17
December 2017

A Novel of PV System Based on Semi active Rectifiers For High-Output Voltage Applications with Isolated Buck-Boost Converters

Kommu Roja & J.Prakash Kumar
[1]M .Tech(Student), St.Martin's Engineering college affiliated to JNTUH Hyderabad Telangana India.
[2]Associate professor, St.Martin's Engineering college affiliated to JNTUH Hyderabad Telangana India.

ABSTRACT- *This paper proposes an isolated buck boost converter with PV system based on semi active rectifiers for high voltage application . In buck boost converter the output voltage either greater than or less than are equal to input voltage based on requirement This systematic method for developing isolated buckboost (IBB) converters is based high output voltage applications , and single-stage power conversion, soft-switching operation, and high-efficiency performance can be achieved with the help of proposed family of converters. A photovoltaic system, also PV system or solar power system, is a power system designed to supply usable solar power by means of photovoltaics An important feature of this stacked structure is the use of low voltage devices while attaining higher number of levels. This will find extensive applications in electric vehicles since direct battery drive is possible. Furthermore, we have to use a family of semiactive rectifiers (SARs) is proposed to serve as the secondary rectification circuit for the IBB converters, it will increase the converter voltage gain and reduce the voltage stresses during rectification process. When the voltage stress are reduced the efficiency is improved by providing of a transformer with a smaller turns ratio and reduced parasitic parameters, by using low-voltage rating MOSFETs and diodes with better switching and conduction performances.*

INTRODUCTION

Isolated dc–dc converters are widely used to meet the in- put/output voltage range and galvanic isolation requirements in the renewable energy and battery discharging applications such as battery-sourced front-end converters for standalone renewable power systems [1], and maximum power point-tracking converters for grid-tied renewable power generation systems [2], [3].

From the perspective of conversion efficiency, an isolated buck-boost (IBB) converter is a promising approach. A flyback converter is a typical IBB converter [15], although its efficiency remains low because of the high-voltage/current stresses on the components and the hard-switching of
the active switch and rectifying diode. Moreover, the flyback converter is only suitable for low-power applications. Fig. 1 shows the diagram of a twoswitch buck-boost converter [16], [17], which is composed of a buck-cell, a boost-cell, and a dc-link inductor.

A family of IBB converters was developed by replacing the nonisolated buck-cell in the nonisolated twoswitch buck-boost converter shown in Fig. 1 with an isolated buck-cell [11]. A wide voltage gain range with flexible control has been achieved with these converters, but the conversion efficiency is hindered by the cascaded two-stage conversion architecture. From the perspective of efficiency, achieving IBB conversion with a single-stage and soft-switching operation is of great interest and represents a potentially valuable research topic.

In addition to the IBB conversion, another significant challenge is the efficient conversion of the low-voltage outputs of renewable energy sources and batteries to a higher voltage, which is necessary because the output voltages of PV arrays, fuel cells, and the batteries employed in renewable power systems are much lower than the dc input voltage of a grid-connected inverter.

In this paper, the concept of semiactive rectifier (SAR) is introduced to alleviate the limitations discussed above. These SARs are derived by merging a half-bridge circuit and a switched-capacitor circuit. The major contribution of this paper is to propose a family of novel IBB converters by employing the SARs as boost-cells. Lower current stresses and isolated buck/boost conversion have been achieved for the proposed SAR-based converters compared with those with passive rectifiers. Owing to the phase shift modulation and capacitive output stage of the SAR, single-stage power conversion, soft-switching operation, and low-voltage stresses on all active switches and diodes can be achieved with the proposed family of converters, and high switching frequency can be adopted to make the input current ripple with high frequency and be easy to be eliminated in the real systems

DERIVATION OF THE IBB DC/DC CONVERTERS

General Structure of the IBB Converter

As shown in Fig. 1, the nonisolated two-switch buck-boost converter is composed of a dc buck-cell, a dc boost-cell, and a dclink inductor.

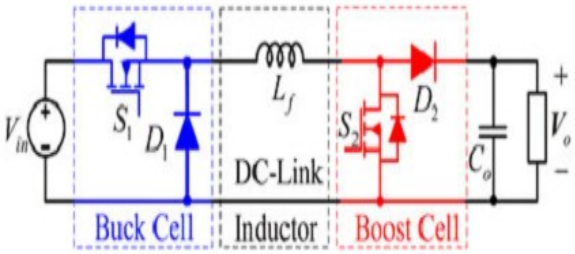

Fig. 1. Diagram of a nonisolated two-switch buck-boost converter.

To construct an IBB converter, a high-frequency transformer can be employed to provide galvanic isolation,

International Journal of Research
Available at https://edupediapublications.org/journals
e-ISSN: 2348-6848
p-ISSN: 2348-795X
Volume 04 Issue-17
December 2017

and the dc-link inductor can be replaced with an ac-link inductor.

Then, a general structure of the IBB converter is obtained and illustrated in Fig. 2. The ac buck-cell in Fig. 2 should be able to generate high frequency ac voltage, vp, which can be realized by full-bridge, half-bridge, and three-level half-bridge switching cells.

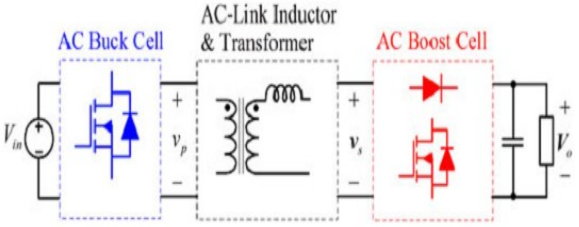

Fig. 2. General structure of the IBB converter.

Some of the implementations of the ac buck-cell have been shown in Fig. 3. By replacing the ac buck-cell in Fig. 2 by the circuit shown in Fig. 3(a)–(d), the primary circuit of the IBB converter can be realized.

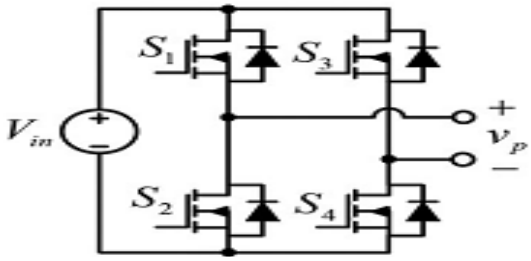

(a)

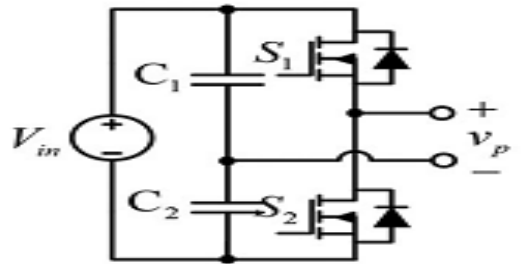

(b)

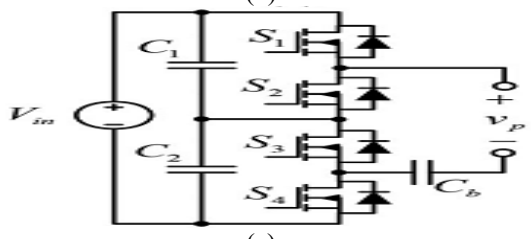

(c)

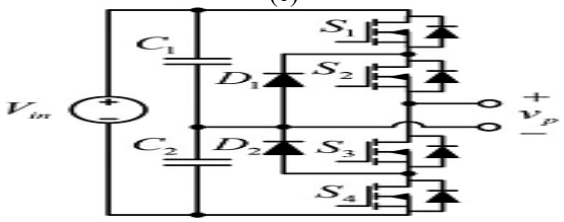

(d)

Fig. 3. Implementation of the ac buck-cell. (a) Full-bridge. (b) Half-bridge. (c) and (d) Three-level.

Realize the ac boost-cell

With SARs The ac boost-cell in Fig. 2 should be able to generate a highfrequency ac voltage vs. There are many possible implementations for the ac boost-cell. To decrease the voltage stress on the devices in the ac boost-cell, a family of SARs is proposed in this section. As shown in Fig. 4, the SAR is developed by merging a symmetrical half-bridge circuit and a boost switched-capacitor circuit [22] with the shared active switches

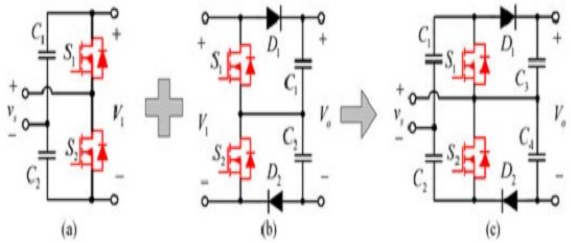

Fig. 4. Derivation of the SAR. (a) Symmetrical half-bridge circuit. (b) Boost switched-capacitor circuit. (c) SAR.

As shown in Fig. 4(c), the proposed SAR is comprised of two active switches S1 and S2, two diodes D1 and D2, and four capacitors C1 − C4. In the SAR, C1 and C2 are the series capacitors, C3 and C4 are the output capacitors. The high-frequency ac voltage vs can be generated by turning ON/OFF S1 and S2 complementarily.

Another two types of SARs can also be developed by merging a symmetrical halfbridge cell and the boost switched-capacitor cells presented in [23] and [24]. The developed SARs have been shown in Fig. 5.

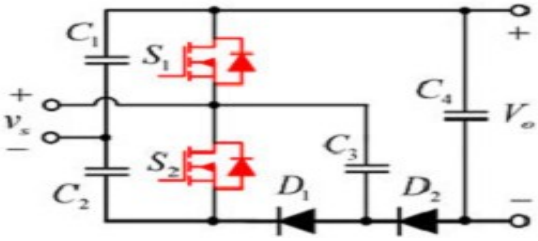

(a)

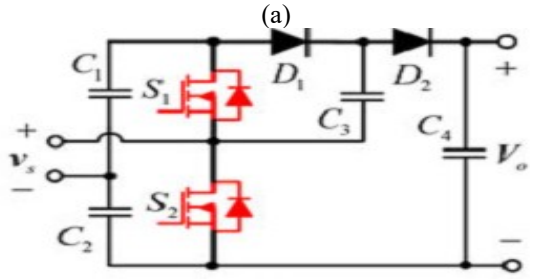

(b)

Fig. 5. Another two types of SARs derived from the symmetrical half-bridge circuit.

The same derivation principles can be applied to the asymmetrical half-bridge topology as well; hence, some

International Journal of Research
Available at https://edupediapublications.org/journals
e-ISSN: 2348-6848
p-ISSN: 2348-795X
Volume 04 Issue-17
December 2017

novel SARs are generated and shown in Fig. 6. It should be noted that the converters given in Fig. 6 are operated similar to the switched capacitor converter and voltage multiplier [23]–[25], and it is important to consider the currents among the capacitors in the real applications.

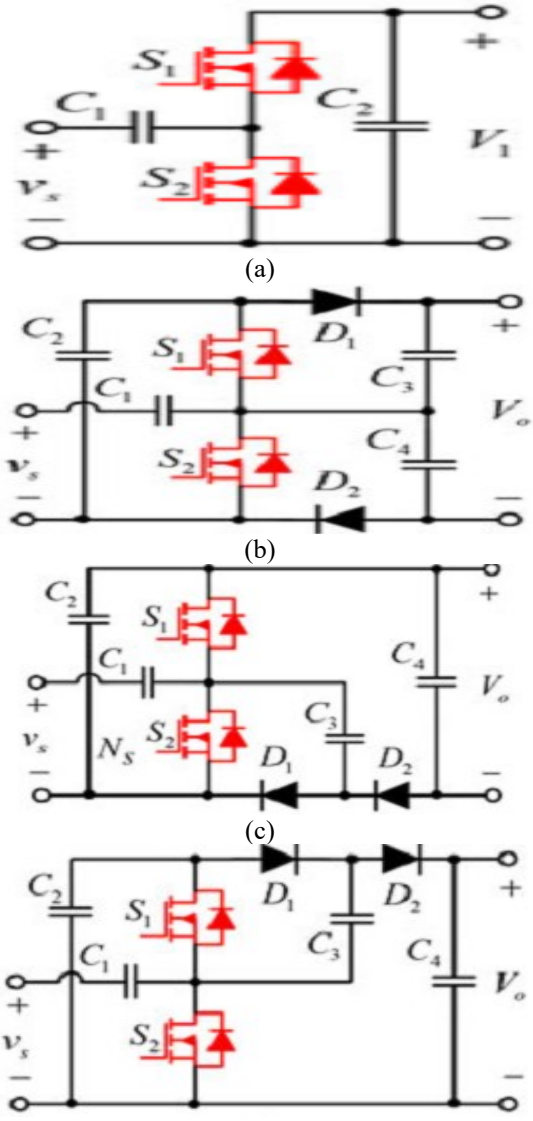

Fig. 6. (a) Asymmetrical half-bridge circuit. (b)–(d) Derived SARs.

Family of IBB Converters

Through replacing the ac buck-cell in Fig. 2 by the circuits shown in Fig. 3, and replacing the ac boost-cell in Fig. 2 by the proposed SARs shown in Figs. 4–6, a family of IBB converters are obtained. Some of the IBB converters are illustrated in Fig. 7, in which the SAR shown in Fig. 4 is employed.

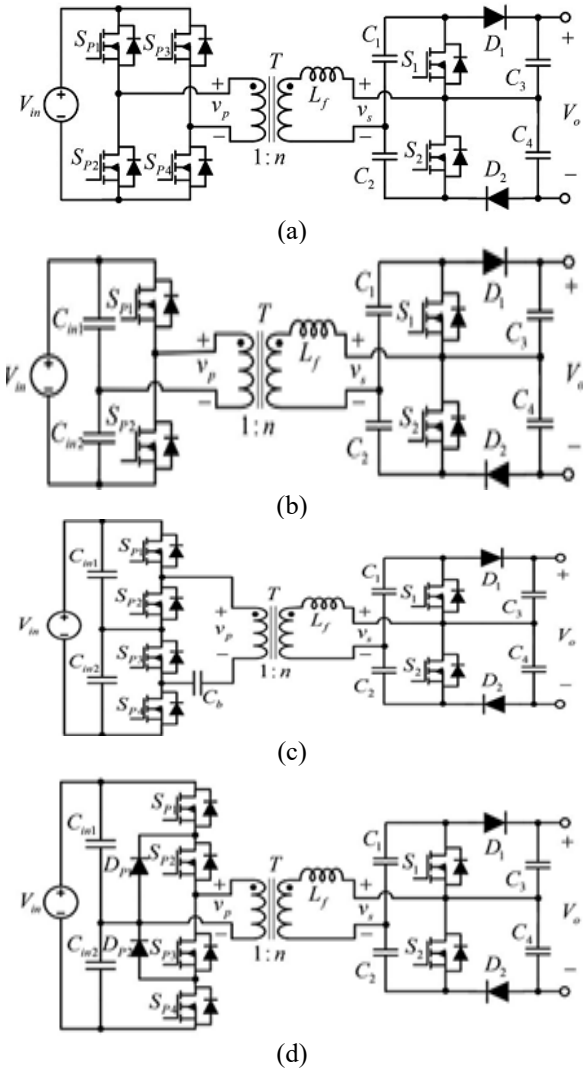

Fig. 7. (a) FB-IBB converter.(b) Half-bridge IBB converter. (c) and (d) Three-level IBB converters.

OPERATIONAL PRINCIPLES OF THE PROPOSED FULL-BRIDGE IBB CONVERTER

A full-bridge IBB (FB-IBB) converter, which is one of the proposed IBB topologies and shown in Fig. 7(a), is taken as an example for analysis. The topology of the FB-IBB is redrawn in Fig. 8, where NP and NS are, respectively, the primary winding and secondary winding of the transformer.

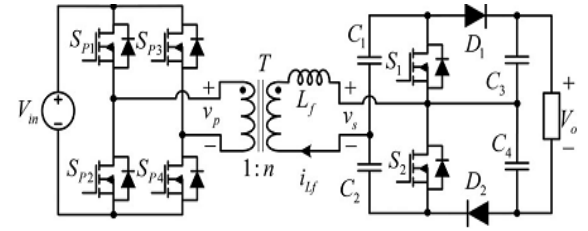

Fig. 8. Topology of the proposed FB-IBB converter.

International Journal of Research
Available at https://edupediapublications.org/journals
e-ISSN: 2348-6848
p-ISSN: 2348-795X
Volume 04 Issue-17
December 2017

It should be noted that, the inductor Lf can be implemented either only with the leakage inductance of the transformer or with an external inductor to achieve the desired value. The normalized voltage gain G is defined as

$$G = \frac{V_O}{4nV_{in}} \qquad (1)$$

where n is the turns ratio of the transformer and n = NS : NP . The converter operates in the boost mode when G ≥ 1, and operates in the buck mode when G < 1. Since there are six active switches in the FB-IBB converter, the control of this converter is very flexible, where PWM control, phase-shift control, or PWM plus phase-shift control can be employed. As illustrated in Fig. 8, the primaryside of the FB-IBB converter is an active full-bridge, and the secondary-side of the converter is a hybrid bridge composed of two active switches and two diodes. All active switches on the primary-side and secondary-side have a constant duty cycle of 0.5. The switches SP 1 and SP 2, SP 3 and SP 4, and S1 and S2 are driven complementary, respectively. The primary-side and secondary-side duty cycles are defined as

$$\begin{cases} D_P = \frac{\varphi_P}{\pi} \\ D_S = \frac{\varphi_S}{\pi} \end{cases} \qquad (2)$$

Boost Mode Operation

In the boost mode, the primary-side duty-cycle is set to be the maximum value DP = 1, which is similar to the nonisolated two-switch buck-boost converter. Thus, the power flow is controlled by changing the secondary-side duty cycle DS . The switches in the primary-side full-bridge produces a square wave voltage waveform indicated as vp in Fig. 8, while the square voltage waveform produced by the secondary-side SAR is indicated as v s in Fig. 8. Fig. 9 shows the operation waveforms of the FB-IBB converter in the boost mode, where fs is the switching frequency.

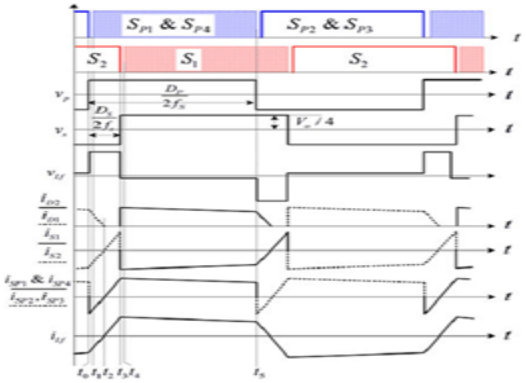

Fig. 9. Switching waveforms of the FB-IBB converter in the boost mode.

To simplify the analysis, the parasitic capacitances of MOSFET are ignored and the transformer is assumed to be ideal. There are ten switching states in one switching period. Due to the symmetry of the circuit, only five states are analyzed here and corresponding equivalent circuits for each switching state are shown in Fig. 10.

State 1[t0, t1] [see Fig. 10(a)]: Before t0, switches SP 2,SP 3,S2 and D1 are ON, and the inductor current iLf < 0.

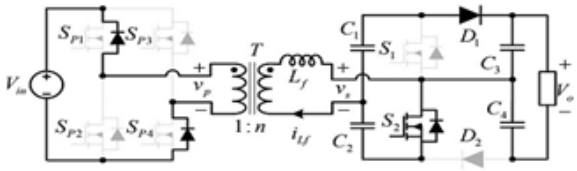

(a)

Fig. 10. Equivalent circuits for each switching state in the boost mode. (a) State 1 [t0, t1].

The input source and the energy stored in the inductor Lf are delivered to the load. CapacitorsC2 andC3 are charged, whereas C1 and C4 are discharged. At t0, SP 2 and SP 3 are turned OFF. The body-diodes of SP 1 and SP 4 begin to conduct due to the energy stored in Lf

$$i_{Lf}(t) = \frac{nV_{in} + \frac{V_O}{4}}{L_f}(t - t_0) + i_{Lf}(t_0) \qquad (3)$$

State 2[t1,t2] [see Fig. 10(b)]: At t1, SP 1 and SP 4 are turned ON with zero voltage switching (ZVS). This state ends when i Lf recovers to zero, and D1 is turned OFF naturally with zero current and without reverse-recovery loss.

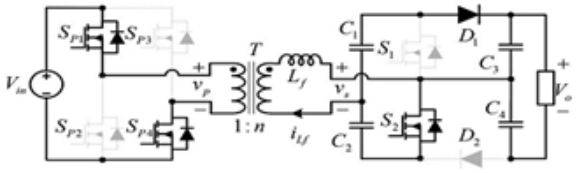

(b)

Fig. 10. Equivalent circuits for each switching state in the boost mode (b) State 2 [t1, t2].

State 3[t2,t3] [see Fig. 10(c)]: At t2, iLf recovers to zero, the inductor L f is charged by the input voltage and the voltage of the capacitor C2.

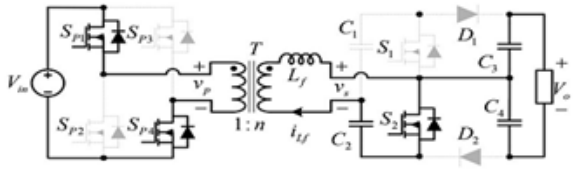

(c)

Fig. 10. Equivalent circuits for each switching state in the boost mode. (c) State 3 [t2, t3].

State 4[t3,t4] [see Fig. 10(d)]: At t3, S2 turns OFF. Since the current i Lf is positive, the body-diode of S1 and the diode D2 begin to conduct. Therefore, the input source and energy stored in the inductor L f are delivered to the load. In this state, the capacitors C1 and C4 are charged, while C2 and C3 are discharged. The inductor current iLf is calculated by

International Journal of Research
Available at https://edupediapublications.org/journals
e-ISSN: 2348-6848
p-ISSN: 2348-795X
Volume 04 Issue-17
December 2017

$$i_{Lf}(t) = \frac{nV_{in} + \frac{V_O}{4}}{L_f}(t - t_3) + i_{Lf}(t_3) \qquad (4)$$

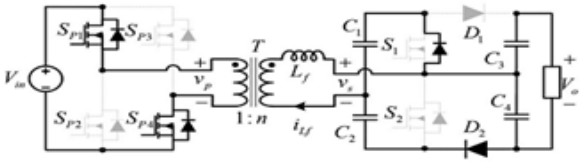

(d)

Fig. 10. Equivalent circuits for each switching state in the boost mode. (d) State 4 [t3, t4].

State 5[t4,t5] [see Fig. 10(e)]: At t4, the switch S1 turns ON with ZVS. The power is transferred to the load from the source continuously in this state. A similar operation occurs in the rest states of the switching period.

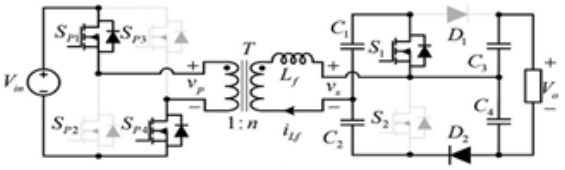

(e)

Fig. 10. Equivalent circuits for each switching state in the boost mode. (e) State 5 [t4, t5].

According to the operational principle analysis, the values of i Lf (t0), iLf (t3), and ΔT2 can be obtained as

$$\begin{cases} i_{Lf}(t_0) = \frac{nV_{in} + (2D_s - 1)\frac{V_0}{4}}{4f_s L_f} \\ i_{Lf}(t_3) = \frac{(2D_s - 1)nV_{in} + \frac{V_0}{4}}{4f_s L_f} \\ \Delta T_2 = t_2 - t_0 = \frac{nV_{in} + (2D_s - 1)\frac{V_0}{4}}{4f_s(nV_{in} + \frac{V_0}{4})} \end{cases} \qquad (5)$$

Ignoring the power loss during the power conversion, the output power can be given b

$$P_O = \frac{D_s(1 - D_s)nV_0V_{in}}{8f_s L_f} \qquad (6)$$

By substituting (1) into (6), the following is obtained:

Buck Mode Operation

In the buck mode, the primary-side duty-cycle is set to be the normalized voltage gain

$$D_P = \frac{V_0}{4nV_{in}} = G \qquad (7)$$

Fig. 11 shows the operation waveforms of the FB-IBB converter in the buck mode when DS > 0. There are 14 switching states in one switching period.

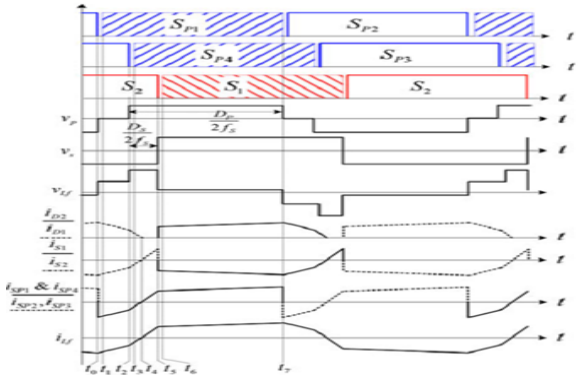

Fig. 11. Switching waveforms of the FB-IBB converter in the buck mode.

Due to the symmetry of the circuit, only seven states are analyzed here and corresponding equivalent circuits for each switching state are shown in Fig. 12.

State 1[t0,t1] [see Fig. 12(a)]: Before t0, switches SP 2,SP 3,S2, and D1 are ON, and the inductor current iLf < 0. The input source and the energy stored in the inductor Lf are delivered to the load.

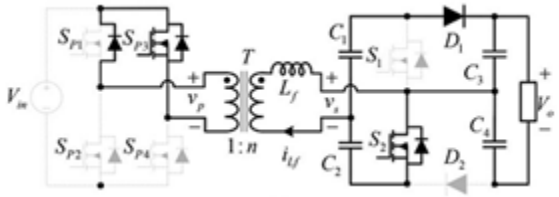

(a)

Fig. 12. Equivalent circuits for each switching state in the buck mode. (a) State 1 [t0, t1].

State 2[t1,t2] [see Fig. 12(b)]: At t1, SP 1 is turned ON wit ZVS. This state ends when the switch SP 3is turned OFF at t2.

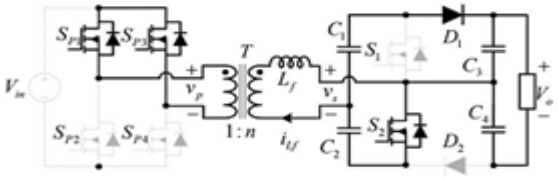

(b)

Fig. 12. Equivalent circuits for each switching state in the buck mode. (b) State 2 [t1, t2].

State 3[t2,t3] [see Fig. 12(c)]: At t2,SP 3 is turned OFF.

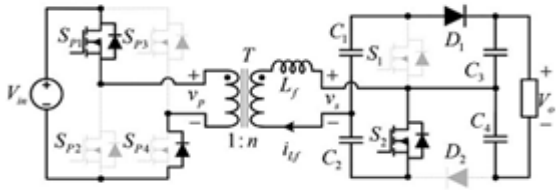

(c)

Fig. 12. Equivalent circuits for each switching state in the buck mode (c) State 3 [t2, t3].

International Journal of Research
Available at https://edupediapublications.org/journals
e-ISSN: 2348-6848
p-ISSN: 2348-795X
Volume 04 Issue-17
December 2017

State 4[t3,t4] [see Fig. 12(d)]: At t3,SP 4 is turned ON with ZVS. This state ends when i Lf recovers to zero, and the diode D1 is OFF naturally with zero current and without reverse recovery loss.

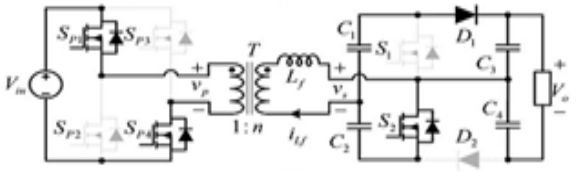

(d)

Fig. 12. Equivalent circuits for each switching state in the buck mode. (d) State 4 [t3, t4].

State 5[t4,t5] [see Fig. 12(e)]: At t4,iLf recovers to zero, the inductor L f is charged by the input voltage and the voltage of the capacitor C2.

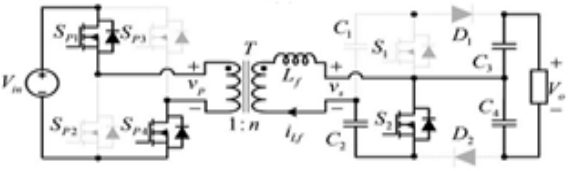

(e)

Fig. 12. Equivalent circuits for each switching state in the buck mode. (e) State 5 [t4, t5].

State 6[t5,t6] [see Fig. 12(f)]: At t5,S2 turns OFF. Since the current i Lf is positive, the body-diode of the switch S1 and the rectifying diode D2 begin to conduct.

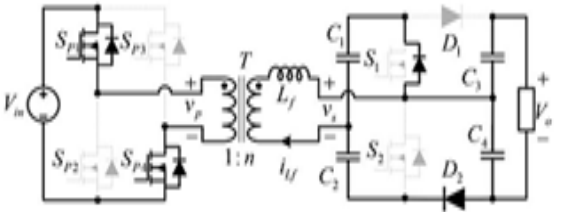

(f)

Fig. 12. Equivalent circuits for each switching state in the buck mode. (f) State 6 [t5, t6].

State 7[t6,t7] [see Fig. 12(g)]: At t6, the switch S1 turns ON with ZVS. The power is transferred to the load from the source continuously in this state.

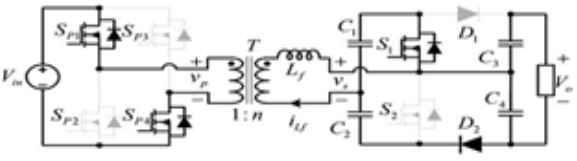

(g)

Fig. 12. Equivalent circuits for each switching state in the buck mode. (g) State 7 [t6, t7]

A similar operation occurs in the rest states of the switching period.

$$P_0 = \frac{[D_s(1-D_S)+0.5(1-D_P)(D_P-2D_S)]nV_0V_{in}}{8f_sL_f} (8$$

It should be noted that, once the primary-side duty-cycle DP is equivalent to the normalized voltage gain G, the output power is not zero even though the secondary-side duty-cycle DS is zero.The operational principle of the proposed FB-IBB converter in buck mode when −0.5(1 − DP) < DS < 0 is omitted here and the output power is given as

$$P_0 = \frac{[D_S+0.5(1-G)]V_O^2}{32f_sL_f} \quad (9)$$

The output power curves versus the secondary-side duty cycle DS with different voltage gains are shown in Fig. 13. According to (7) and as shown in Fig. 13, if the converter works in the boost mode, the maximum output power occurs when the secondary side duty-cycle DS is equal to 0.5.

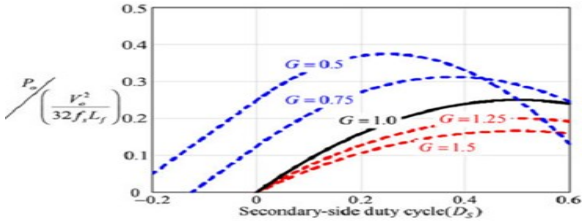

Fig. 13. Output power curves versus the secondary-side duty cycle.

PERFORMANCE ANALYSIS AND COMPARISON

A.Normalized Voltage Gain

The output power Po can be calculated as

$$P_0 = \frac{V_0^2}{R_0} (10)$$

The normalized voltage gain curves versus the secondary side duty cycle DS are plotted in Fig. 14.

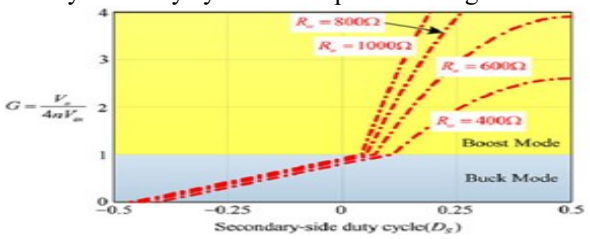

Fig. 14. Normalized voltage gain versus the secondary-side duty cycle.

Soft-Switching Performance

According to the operational principles of different modes, the ZVS operation can be achieved for all active switches owing to the phase-shift control strategy, while zero current switching (ZCS) can be realized for all diodes. Once the body diode of the MOSFET is in the ON-state before turning ON the MOSFET, ZVS is achieved.

Fig. 15. In order to discharge Coss to zero during the dead-time and realize the ZVS for primary-side switches, the following condition is required:

International Journal of Research
Available at https://edupediapublications.org/journals
e-ISSN: 2348-6848
p-ISSN: 2348-795X
Volume 04 Issue-17
December 2017

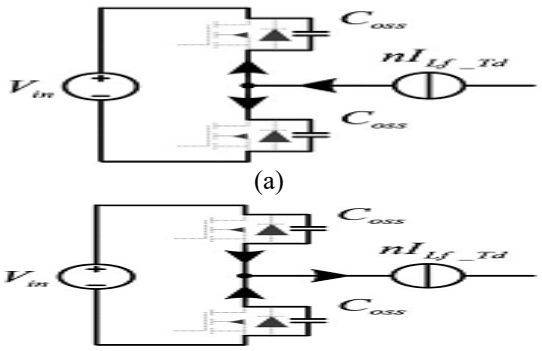

Fig. 15. Equivalent circuit during the dead-time. (a) SP 1 or SP 3 is discharged. (b) SP 2 or SP 4 is discharged.

By comparing the ZVS conditions given in (19) and (21), it can be found that the ZVS range is narrowed due to the influence of output capacitances. Using the same analysis method, the ZVS conditions for primary-side and secondary-side switches in different operation modes are shown in Table I

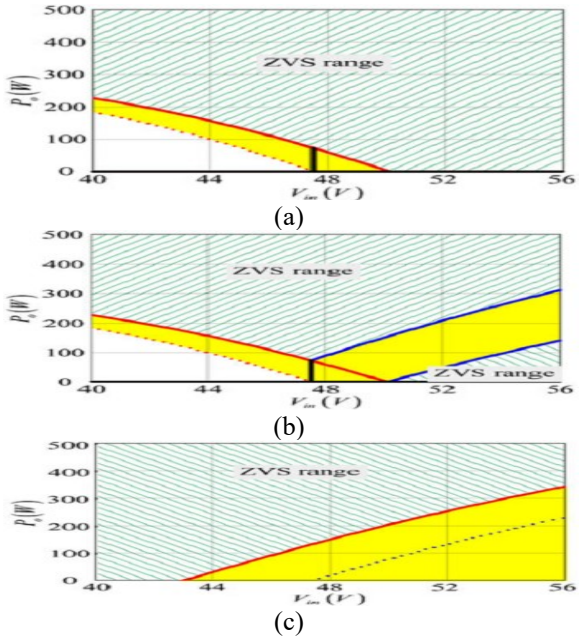

Fig. 16. ZVS range. (a) SP 1 and SP 2 . (b) SP 3 and SP 4 . (c) S1 and S2 .

TABLE I
Zvs Conditions

	$S_{P1}andS_{P2}$	$S_{P3}andS_{P4}$	S_1andS_2
BOOST MODE	$D_S \geq \frac{4f_sL_fC_{oss}}{n^2T_dG} + \frac{G-1}{2G}$		$D_S \geq \frac{8f_sL_fC_{oss}}{T_d} + \frac{G-1}{2}$
BACK MODE	$D_S \geq \frac{4f_sL_fC_{oss}}{n^2T_d} + \frac{G^2-1}{2G}$	$D_S \geq \frac{4f_sL_fC_{oss}}{n^2T_d}\frac{1}{G}$ $D_S \leq -\frac{4f_sL_fC_{oss}}{n^2T_d}$	$D_S \geq \frac{8f_sL_fC_{oss}}{T_d}$

1) Turns Ratio of Transformer: According to previous analysis, the proposed converter has better soft-switching performance while operating with G = 1 and is getting worse when G is far away from 1. Therefore, it is recommended that the turns ratio of the transformer is designed to ensure the operation with G around 1.

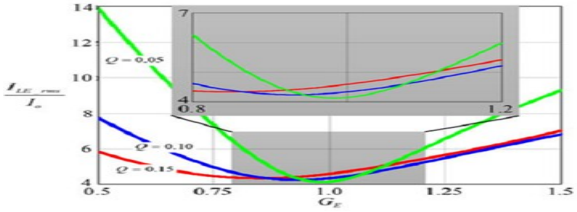

Fig. 17. Normalized inductor RMS currents versus normalized voltage gain with different characteristic factors.

Performance Comparison Between the Proposed SAR-Based FB-IBB Converter and the Full-bridge Converter With SVQR

Compared with the full-bridge converter with the symmetrical voltage quadrupler rectifier (SVQR) proposed in [20] (shown in Fig. 18), the proposed SAR-based FB-IBB converter offers some better performances.

The normalized voltage gain curves versus the primary-side duty cycle DP are shown in Fig. 18. These curves are plotted

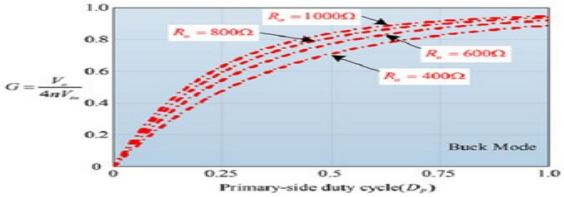

Fig. 18. Normalized voltage gain of the full-bridge converter with SVQR.

By comparing the normalized voltage gain curves given in Figs. 14 and 19, it can be concluded that the higher output voltage gain can be achieved by the proposed SAR-based FB-IBB converter than the full-bridge converter with SVQR.

Inductor Current Value Comparison:

According to the analysis mentioned previously, the inductor Lf is known as a key component both in the proposed converter and the full-bridge converter with SVQR.

International Journal of Research
Available at https://edupediapublications.org/journals
e-ISSN: 2348-6848
p-ISSN: 2348-795X
Volume 04 Issue-17
December 2017

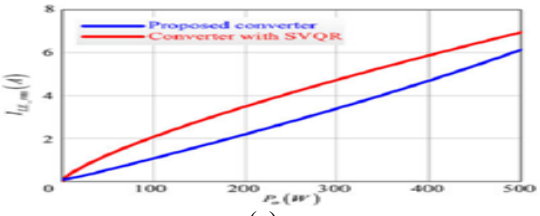

(a)

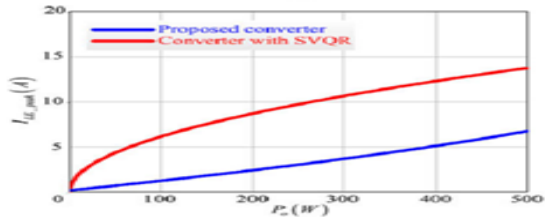

(b)

Fig. 19. Inductor current comparison. (a) RMS value. (b) Peak value.

The comparison of inductor currents between the proposed converter and the full-bridge converter with SVQR is shown in Fig. 19. These curves are plotted under the conditions given in Table II.

TABLE II
Inductor Current Value Comparison Conditions

Parameter	Proposed converter	Converter with SVQR
Input voltage (V_{in})	40-56v	40-56v
Output voltage (V_o)	380V	380V
Switching frequency	100KHz	100KHz
Turns ratio of transformer	1:2	1:3
Inductor L_f	15μH	9μH

The conduction loss of power switches and the copper loss of transformer/inductors are directly affected by the RMS values of inductor currents, and the current stresses on power switches depend on the peak values of inductor currents. Therefore, the power switches of the full-bridge converter with SVQR, especially the primary-side switches suffer higher current stresses and have higher conduction loss.

PV SOURCE

Photovoltaics (PV) covers the conversion of light into electricity using semiconducting materials that exhibit the photovoltaic effect, a phenomenon studied in physics, photochemistry, and electrochemistry. The dynamic model of PV cell is shown in below Fig.21.

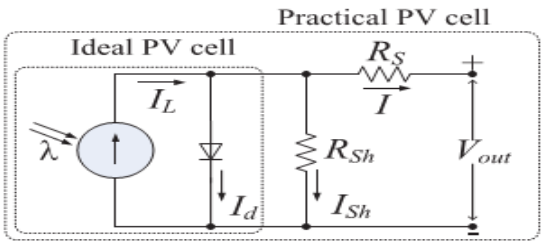

Fig 20.Equivalent electrical circuit of the PV cell.

The basic equation describing the I -V characteristic of a practical PV cell is

$$I = I_L - I_d - I_{sh} = I_L - I_D\left[e^{\frac{QV_{oc}}{AKT}-1}\right] - \frac{V_{out}+IR_S}{R_{Sh}} \quad (8)$$

where I D is the saturation current of the diode, Q is the electron charge, A is the curve fitting constant (or diode emission factor), K is the Boltzmann constant and T is the temperature on absolute scale. PV systems convert light directly into electricity and shouldn't be confused with other technologies, such as concentrated solar poweror solar thermal, used for heating and cooling.

Photovoltaics (PV) is a term which covers the conversion of light into electricity that exhibit the photovoltaic effect, a phenomenon studied in physics, photochemistry, and electrochemistry

Photovoltaic (PV) power generation is becoming more promising since the introduction of the thin film PV technology due to its lower cost, excellent high temperature performance, low weight, flexibility, and glass-free easy installation

SIMULATION VERIFICATION

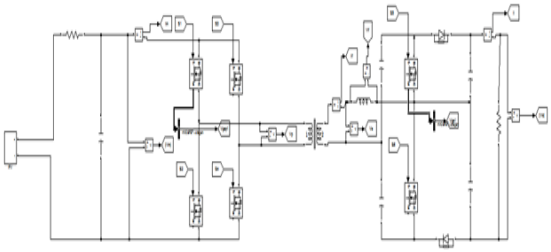

Fig 21 Simulation of Block diagram

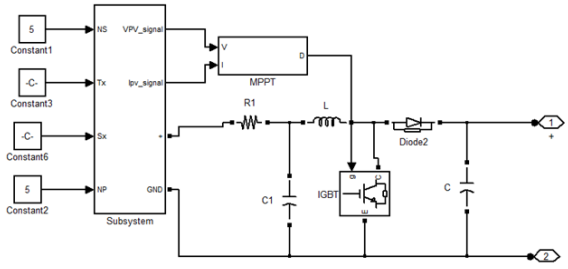

Fig 22 Simulation diagram of PV system

Figs.23 and 24 show the simulation waveforms of the proposed converter in the boost mode. The waveforms in

International Journal of Research
Available at https://edupediapublications.org/journals
e-ISSN: 2348-6848
p-ISSN: 2348-795X
Volume 04 Issue-17
December 2017

Fig. 23 are tested under 40-V input voltage with the normalized voltage gain G > 1.

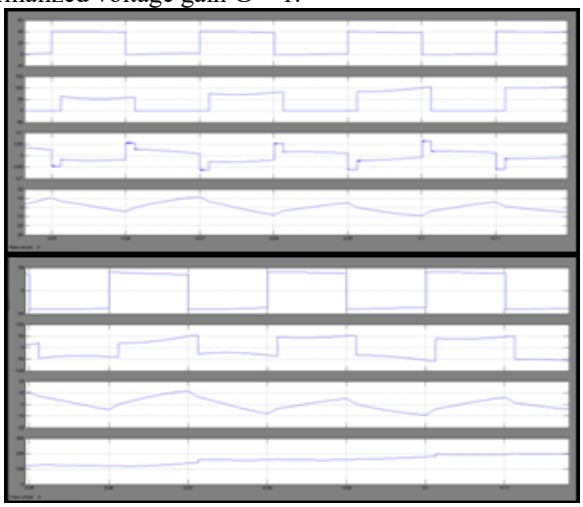

Fig. 23. Simulation waveforms of the proposed converter when the voltage gain G > 1. (a) Driving voltages of SP 1 and S1 (vGSP1 and vGS1), voltage applied on the inductor (vLf) and current through the inductor (iLf). (b) Square wave voltages on primary-side and secondary-side (vp , vs), and iLf

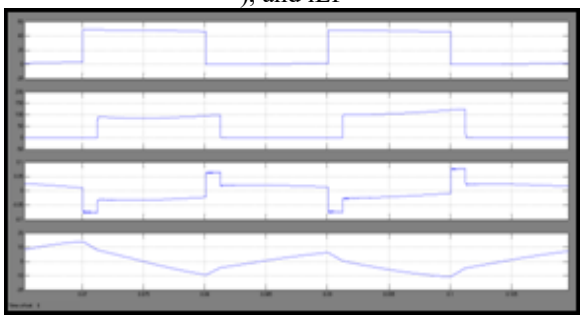

Fig. 24. Simulation waveforms of the proposed converter when the voltage gain G = 1. (a) Driving voltages of SP 1 and S1 (vGSP1 and vGS1), voltage applied on the inductor (vLf), and current through the inductor (iLf), (b) Square wave voltages on primary-side and secondary-side (vp , vs), and iLf .

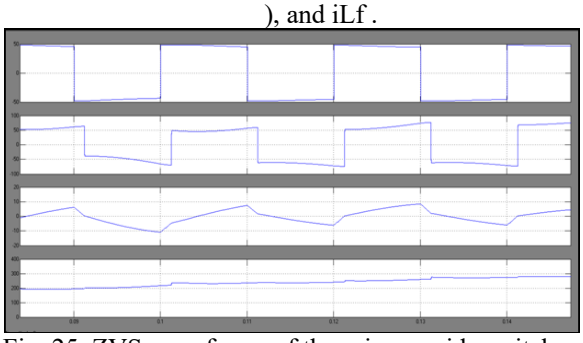

Fig. 25. ZVS waveforms of the primary-side switch and the secondary-side switch of the proposed converter in the boost mode.

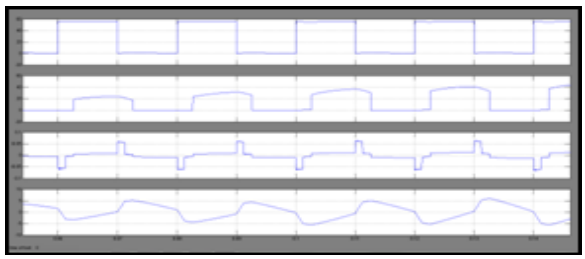

Fig. 26. waveforms of the proposed converter when the voltage gain G < 1. (a) Driving voltages of SP 1 , SP 4 , and S1 (vGSP1 , vGSP4 , and vGS1), and current through the inductor (iLf). (b) Driving voltages of SP 1 (vGSP1), square wave voltages on primary-side and secondary-side (vp , vs), and i Lf

The driving and drain–source voltages of the proposed converter in the buck mode are shown in Fig. 27. It can be seen that, ZVS has been achieved for all the primary-side and secondary-side switches.

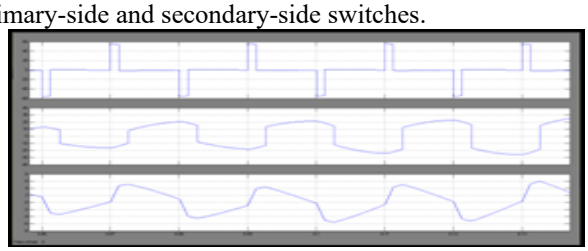

Fig. 27. ZVS waveforms of the proposed converter in the buck mode. (a) driving and drain–source voltages of SP 1 , and SP 4 (vGSP1 , vDSP1 , vGSP4 , and vDSP4). (b) Driving and drain–source voltages of SP 1 , and S1 (vGSP1, vDSP1, vGS1 , and vDS1).

Fig. 28 shows the simulation waveforms of the full-bridge converter with SVQR, which are tested under 48-V input voltage.

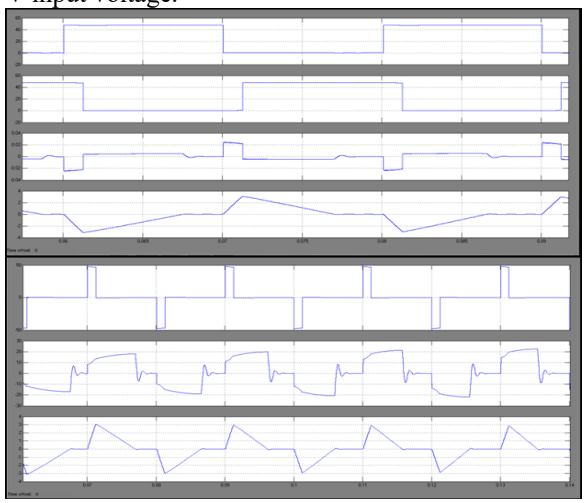

Fig. 28. waveforms of the full-bridge converter with SVQR. (a) Driving voltages of SP 1 and SP 4 (vGSP1 and vGSP4), voltage applied on the inductor (vLf), and current through the inductor (iLf). (b) square wave voltages on primary-side and secondary-side (vp , vs), and iLf .

CONCLUSION

In this paper proposed an novel family of IBB converters with PV system has been implemented for high output voltage based on active rectifiers for reducing of voltage stresses. PV system has having specific advantages as an energy source its operation does not produce the pollution and no greenhouse gas emissions once installed, it shows simple scalability in respect of power needs and silicon has large availability in the Earth's crust .The IBBs are based on the nonisolated two-switch buck-boost converter, and generated by replacing the dc buck-cell and boost-cell in the nonisolated two-switch buck-boost converter by an ac buck-cell and boost-cell. SARs are developed by merging a half-bridge circuit and a switched capacitor circuit, and used as the boost-cell in the IBB converter for high-output voltage applications. The voltage stresses on the devices in the SAR are reduced significantly, and hence, low voltage rating devices with better conduction and switching performance have been used to improve efficiency and also using ZVS and ZCS respectively, by adopting the phase-shift modulation.

REFERENCES

[1] R. Gules, J. De Pellegrin Pacheco, H. Leaes Hey, and J. Imhoff, "A ˜ maximum power point tracking system with parallel connection for PV stand-alone applications," IEEE Trans. Ind. Electron., vol. 55, no. 7, pp. 2674–2683, Jul. 2008.

[2] J. Zeng, W. Qiao, L. Qu, and Y. Jiao, "An isolated multiport DC-DC converter for simultaneous power management of multiple different renewable energy sources," IEEE J. Emerg. Sel. Topics Power Electron., vol. 2, no. 1, pp. 70–78, Mar. 2014.

[3] H. Wu, K. Sun, R. Chen, H. Hu, and Y. Xing, "Full-Bridge three-port converters with wide input voltage range for renewable power systems," IEEE Trans. Power Electron., vol. 27, no. 9, pp. 3965–3974, Sep. 2012.

[4] Z. Guo, D. Sha, and X. Liao, "Input-series-output-parallel phase-shift full-bridge derived DC-DC converters with auxiliary LC networks to achieve wide zero-voltage switching range," IEEE Trans. Power Electron., vol. 29, no. 10, pp. 508–513, Oct. 2014

[5] H. Wu and Y. Xing, "Families of forward converters suitable for wide input voltage range applications," IEEE Trans. Power Electron., vol. 29, no. 11, pp. 6006–6017, Nov. 2014.

[6] D. S. Gautam, F. Musavi, W. Eberle, and W. G. Dunford, "A zero-voltage switching full-bridge DC-DC converter with capacitive output filter for plug-in hybrid electric vehicle battery charging," IEEE Trans. Power Electron., vol. 28, no. 12, pp. 5728–5735, Dec. 2013.

[7] Y. Wang, W. Liu, H. Ma, and L. Chen, "Resonance analysis and softswitching design of isolated boost converter with coupled inductors for vehicle inverter application," IEEE Trans. Power Electron., vol. 30, no. 3, pp. 1383–1392, Mar. 2015.

[8] H. Kim, C. Yoon, and S. Choi, "An improved current-fed ZVS isolated Boost converter for fuel cell applications," IEEE Trans. Power Electron., vol. 25, no. 9, pp. 2357–2364, Sep. 2010.

[9] Y. Zhao, W. Li, Y. Deng, and X. He, "Analysis, design, and experimentation of an isolated ZVT boost converter with coupled inductors," IEEE Trans. Power Electron., vol. 26, no. 2, pp. 541–550, Feb. 2011.

[10] H. Keyhani and H. A. Toliyat, "Partial-resonant buck-boost and flyback DC-DC converters," IEEE Trans. Power Electron., vol. 29, no. 8, pp. 4357–4365, Aug. 2014.

KOMMU ROJA

Completed B.Tech in Electrical &Electronics Engineering in 2015 from KAKATIYA UNIVERSITY,WARNGAL and pursuing M .Tech from St.Martin's Engineering college affiliated to JNTUH Hyderabad Telangana India PES(Power Electronic System)Engineering as specialization **Area of interest includes power electronic systems**

J.PRAKASH KUMAR

J.PRAKASH KUMAR was born in Hyderabad, India. He received the B.Tech and M.Tech degrees in Electrical Engineering from J N T University, Hyderabad, India. He is working as an Assoc.Prof in EEE Dept. in St.Martin's Engg. College. His research interest Power System Protection, Monitoring and Control development in Digital Protective Relays and Smart grid, Power Electronics and Control Systems.